Inorganic Chemistry

Article

pubs.acs.org/IC

New Series of Dinuclear Ruthenium(II) Complexes Synthesized Using Photoisomerization for Efficient Water Oxidation Catalysis

Masanari Hirahara,[†] Sho Nagai,[†] Kosuke Takahashi,[†] Kenji Saito,[†] Tatsuto Yui,[†] and Masayuki Yagi*[,†,§]

[†]Department of Materials Science and Technology, Faculty of Engineering, Niigata University, 8050 Ikarashi-2, Niigata 950-2181, Japan

[§]Precursory Research for Embryonic Science and Technology (PRESTO), Japan Science and Technology Agency (JST), 4-1-8 Honcho, Kawaguchi, Saitama 332-0012, Japan

Supporting Information

ABSTRACT: A new series of *proximal,proximal*-$[Ru_2(tpy)_2(L)XY]^{n+}$ (*p,p*-**Ru_2XY**, tpy = 2,2′:6′,2″-terpyridine, L = 5-phenyl-2,8-di(2-pyridyl)-1,9,10-anthyridine, X and Y = other coordination sites) were synthesized using photoisomerization of a mononuclear complex. The *p,p*-**Ru_2XY** complexes undergo unusual reversible bridge-exchange reactions to generate *p,p*-**$Ru_2(\mu\text{-Cl})$**, *p,p*-**$Ru_2(\mu\text{-OH})$**, and *p,p*-**$Ru_2(OH)(OH_2)$** with μ-Cl, μ-OH, as well as hydroxo and aquo ligands at X and Y sites of *p,p*-**Ru_2XY**, respectively. The geometric and electronic structures of these complexes were characterized based on UV−vis and ^{1}H NMR spectra, X-ray crystallography, and density functional theory (DFT) calculations. ^{1}H NMR data showed C_2 symmetry of *p,p*-**$Ru_2(OH)(OH_2)$** with the distorted L chelate and nonequivalence of two tpy ligands, in contrast to the C_{2v} symmetry of *p,p*-**$Ru_2(\mu\text{-Cl})$** and *p,p*-**$Ru_2(\mu\text{-OH})$**. However, irrespective of the lower symmetry, *p,p*-**$Ru_2(OH)(OH_2)$** is predominantly formed in neutral and weakly basic conditions due to the specially stabilized core structure by multiple hydrogen-bond interactions among aquo, hydroxo, and backbone L ligands. The electrochemical data suggested that *p,p*-**$Ru_2(OH)(OH_2)$** (Ru^{II}−OH:Ru^{II}−OH_2) is oxidized to the Ru^{III}−OH:Ru^{III}−OH state at 0.64 V vs saturated calomel electrode (SCE) and further to Ru^{IV}═O:Ru^{IV}—OH at 0.79 V by successive 1-proton-coupled 2-electron processes at pH 7.0. The cyclic voltammogram data exhibited that the *p,p*-**$Ru_2(OH)(OH_2)$** complex works more efficiently for electrocatalytic water oxidation, compared with a similar mononuclear complex *distal*-$[Ru(tpy)(L)OH_2]^{2+}$ (*d*-**$RuOH_2$**) and *p,p*-**$Ru_2(\mu\text{-Cl})$** and *p,p*-**$Ru_2(\mu\text{-OH})$**, showing that the *p,p*-**Ru_2** core structure with aquo and hydroxo ligands is important for efficient electrocatalytic water oxidation. Bulk electrolysis of the *p,p*-**$Ru_2(OH)(OH_2)$** solution corroborated the electrocatalytic cycle involving the Ru^{III}−OH:Ru^{III}−OH state species as a resting state. The mechanistic insight into O−O bond formation for O_2 production was provided by the isotope effect on electrocatalytic water oxidation by *p,p*-**$Ru_2(OH)(OH_2)$** and *d*-**$RuOH_2$** in H_2O and D_2O media.

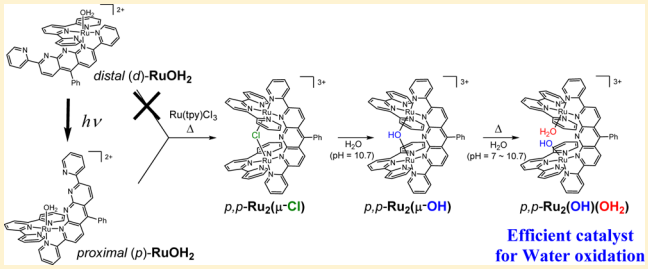

INTRODUCTION

The ruthenium(II) complexes with polypyridyl ligands have been extensively studied due to the unique photochemical and photophysical properties such as photoluminescence,[1−3] photoredox,[4,5] photosubstitution,[6−9] and photoisomerization[10−16] processes typically involving a photoexcited triplet metal-to-ligand charge transfer (^{3}MLCT) state. Recently, we reported stoichiometric photoisomerization of *distal*-$[Ru(tpy)(pynp)OH_2]^{2+}$[17] (tpy = 2,2′:6′,2″-terpyridine, pynp = 2-(2-pyridyl)-1,8-naphthyridine) to *proximal*-$[Ru(tpy)(pynp)OH_2]^{2+}$ (Scheme 1),[15,16] which had not previously been characterized for polypyridyl ruthenium(II) aquo complexes. We first challenge extending the photoisomerization of ruthenium(II) aqua complexes to strategic synthesis of a target molecule being difficult to be synthesized by conventional thermal reactions so far.

Water splitting by sunlight into molecular hydrogen and oxygen in artificial photosynthesis is a promising technology to settle energy and environmental issues. In this context, much

Scheme 1. Photoisomerization of *Distal*-$[Ru(tpy)(pynp)OH_2]^{2+}$ to *Proximal*-Isomer

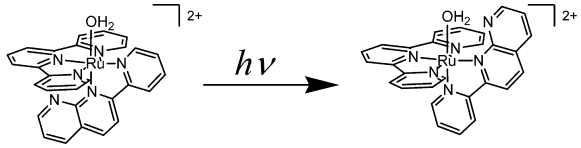

distal-$[Ru(tpy)(pynp)OH_2]^{2+}$ *proximal*-$[Ru(tpy)(pynp)OH_2]^{2+}$

effort has been paid for development of molecular catalysts for water oxidation inspired by the *oxygen-evolving complex* in photosystem II.[18−21] The polypyridyl ruthenium aquo complexes have been extensively studied as water oxidation catalysts.[15,22−33] A few reports pointed out O_2 production by a radical coupling mechanism between the high-valent

Received: June 4, 2015
Published: July 22, 2015

DOI: 10.1021/acs.inorgchem.5b01264
Inorg. Chem. 2015, 54, 7627−7635

ruthenium oxoes (Ru^{V}=O, formally the same as Ru^{IV}–$O^{\bullet}$).[24,30,34] This encourages us to design a dinuclear complex with aquo ligands close to each other, which is expected to prompt O–O bond formation by intramolecular radical coupling of high-valent ruthenium oxoes derived from the aquo ligands. Herein we report the unique synthesis of a new series of *proximal,proximal*-$[Ru_2(tpy)_2(L)XY]^{3+}$ (L = 5-phenyl-2,8-di(2-pyridyl)-1,9,10-anthyridine, X and Y = the other coordination sites; denoted as ***p,p*-Ru$_2$XY**) dinuclear ruthenium(II) complexes using photoisomerization of a mononuclear complex. The ***p,p*-Ru$_2$XY** complexes undergo unusual reversible bridge-exchange reactions to generate derivatives of ***p,p*-Ru$_2$(μ-Cl)**, ***p,p*-Ru$_2$(μ-OH)**, and ***p,p*-Ru$_2$(OH)(OH$_2$)** with μ-Cl, μ-OH, as well as hydroxo and aquo ligands at X and Y sites of ***p,p*-Ru$_2$XY**, respectively. The electrocatalytic water oxidation by these derivatives and a similar mononuclear complex was examined in homogeneous solution. The isotope effects on the electrocatalysis in H_2O and D_2O media will be reported to provide mechanistic insight into O–O bond formation for O_2 production.

EXPERIMENTAL SECTION

Materials. Ru(tpy)Cl_3[35] and L[36] were prepared as previously described. Deuterated solvents were purchased from JUNSEI Chem. Co. All other reagents were purchased and used without further purification.

Syntheses and Characterization of Ruthenium Complexes. *1. Distal-[Ru(tpy)(L)Cl]Cl (d-[**RuCl**]Cl).* Ru(tpy)Cl_3 (44 mg, 0.10 mmol), L (41 mg, 0.10 mmol), LiCl (20 mg), EtOH (15 mL), and ascorbic acid (30 mg, 0.17 mmol) were refluxed for 4 h. The green-colored mixture was evaporated to ca. 1 mL and then filtered. To the filtrate was added chloroform (30 mL) and Na_2SO_4. The solution was filtered to remove deposited LiCl and Na_2SO_4 and then evaporated to dryness. The solid residue dissolved in an eluent containing 90% chloroform and 10% methanol passed through a silica gel column. The first green band was collected and evaporated to dryness. Single crystals suitable for X-ray structure analysis were obtained by slow evaporation of methanol and an aqueous solution of *d*-[**RuCl**]Cl and LiCl. Yield: 47 mg (59%). Anal. Calcd for *d*-[**RuCl**]Cl·5H_2O, $C_{42}H_{28}N_8Cl_2Ru·5.5H_2O$: C, 55.08; H, 4.29; N, 12.24. Found: C, 55.17; H, 4.22, N, 12.09. ^{1}H NMR (399.937 MHz, 20% CD_3OD and 80% $CDCl_3$) δ (ppm): 10.52 (dd, *J* = 5.7, 0.9 Hz, 1H, H_i), 9.05 (d, *J* = 8.2 Hz, 1H, H_f), 8.74 (ddd, *J* = 4.8, 1.7, 0.9 Hz, 1H, $H_{i'}$), 8.65 (d, *J* = 7.9 Hz, 1H, $H_{f'}$), 8.47 (d, *J* = 9.2 Hz, 1H, H_d), 8.44–8.37 (m, 3H, $H_{d'}$ and H_k), 8.31 (dt, *J* = 8.0, 1.5 Hz, 1H, H_g), 8.21–8.16 (m, 1H, $H_{g'}$), 8.14 (d, *J* = 8.0 Hz, 2H, H_l), 8.07 (t, *J* = 8.1 Hz, 1H, H_j), 8.00 (d, *J* = 9.1 Hz, 1H, H_e), 7.97 (d, *J* = 9.0 Hz, 1H, $H_{e'}$), 7.91 (ddd, *J* = 7.3, 5.7, 1.2 Hz, 1H, H_h), 7.66 (dt, *J* = 7.9, 1.5 Hz, 2H, H_m), 7.58–7.48 (m, 4H, H_a, H_b, and $H_{h'}$), 7.41 (dd, *J* = 5.6, 0.8 Hz, 2H, H_n), 7.21–7.15 (m, 2H, H_c), 7.11–7.05 (m, 2H, H_o). ^{13}C NMR (175.992 MHz, 20% CD_3OD and 80% $CDCl_3$) δ (ppm): 164.79 (C_i), 162.57 ($C_{i'}$), 160.19 (C_s), 157.55 (C_r), 157.30 ($C_{j'}$), 157.20 (C_k), 155.03 ($C_{k'}$), 154.97 (C_j), 153.96 (C_o), 152.52 (C_e), 151.66 (C_w), 149.57 ($C_{o'}$), 137.01 ($C_{m'}$), 136.60 (C_u), 136.49 ($C_{h'}$), 136.19 (C_m), 135.17 (C_h), 133.67 (C_p), 132.81 (C_d), 129.99 (C_c), 129.74 (C_a), 128.95 (C_b), 127.13 (C_n), 126.87 (C_l), 126.40 (C_v), 125.57 ($C_{n'}$), 122.99 ($C_{l'}$), 122.63 (C_t), 121.64 (C_q), 121.41 ($C_{f'}$), 121.02 ($C_{g'}$), 120.41 (C_f), 119.00 (C_g). UV–vis (λ, nm (ε, 10^3 mol^{-1} L cm^{-1}) in methanol): 241 (50.0), 282 (44.0), 297 (44.0), 315 (36.0), 375 (31.0), 472 (4.1), 642 (6.3). ESI MS (solvent: methanol), *m*/*z* (calcd): 781.1 (781.1, *d*-[**RuCl**]$^+$). ^{1}H and ^{13}C NMR, COSY, HMQC, HMBC, and ESI MS spectra are shown in Figure S1, Supporting Information.

*2. Distal-[Ru(tpy)(L)(OH$_2$)](NO$_3$)$_2$ (d-[**RuOH$_2$**](NO$_3$)$_2$).* To a 10 mL round-bottom flask were added *d*-[**RuCl**]Cl (16.3 mg, 0.020 mmol), 3 mL of water, and an aqueous solution of 0.1 M $AgNO_3$ (0.40 mL, 0.040 mmol). The reaction mixture was stirred at 80 °C for 4 h in the dark and filtered. An aqueous solution of $NaNO_3$ was added to the filtrate, and a green precipitate was filtered and dried in vacuum. Yield: 15.9 mg (90%). Anal. Calcd for *d*-[**RuOH$_2$**](NO$_3$)$_2$·H_2O, $C_{42}H_{30}N_{10}O_7Ru·H_2O$: C, 55.69; H, 3.56; N, 15.46. Found: C, 55.45; H, 3.39, N, 15.20. ^{1}H NMR (699.837 MHz, 80% CD_3OD and 20% D_2O) δ (ppm): 9.73 (d, *J* = 5.2 Hz, 1H, H_i), 8.99 (d, *J* = 8.4 Hz, 1H, H_f), 8.63 (d, *J* = 8.3 Hz, 2H, H_k), 8.53–8.47 (m, 1H, $H_{i'}$), 8.44 (t, *J* = 8.0 Hz, 1H, H_g), 8.32–8.23 (m, 4H, $H_{f'}$, H_j, and H_l), 8.18 (d, *J* = 9.3 Hz, 1H, H_d), 8.15–8.09 (m, 2H, $H_{g'}$ and H_h), 7.62 (t, *J* = 7.8 Hz, 2H, H_m), 7.50 (dd, *J* = 7.0, 5.4 Hz, 1H, $H_{h'}$), 7.49–7.43 (m, 3H, H_e and H_o), 7.27–7.19 (m, 2H, H_a and $H_{d'}$), 7.07 (t, *J* = 6.6 Hz, 2H, H_n), 6.88 (t, *J* = 7.5 Hz, 2H, H_b), 6.29 (d, *J* = 8.6 Hz, 1H, $H_{e'}$), 5.98 (d, *J* = 6.8 Hz, 2H, H_c). ^{13}C NMR (175.992 MHz, 20% CD_3OD and 80% D_2O) δ (ppm): 167.20 (C_i), 162.56 ($C_{i'}$), 161.28 (C_s), 159.12 (C_r), 158.07 ($C_{k'}$), 157.51 (C_k), 155.10 ($C_{j'}$), 154.34 (C_j), 153.69 (C_w), 152.87 (C_o), 152.87 (C_e), 150.31 ($C_{o'}$), 139.07 (C_u), 138.98 ($C_{m'}$), 138.09 (C_m), 136.93 (C_p), 136.12 (C_h), 135.88 ($C_{h'}$), 132.46 (C_d), 130.63 (C_a), 130.34 (C_c), 129.46 (C_b), 129.33 (C_n), 128.56 (C_l), 128.24 (C_v), 127.39 ($C_{n'}$), 124.35 ($C_{l'}$), 124.12 (C_t), 123.75 (C_q), 120.76 ($C_{g'}$), 120.62 (C_f, $C_{f'}$), 120.07 (C_g). UV–vis (λ, nm (ε, 10^3 mol^{-1} L cm^{-1}) in water): 238 (35.0), 282 (36.0), 294 (38.0), 387 (29.0), 458 (3.3), 614 (5.7). ESI MS (solvent: methanol) (*m*/*z*): 373.1 ([*d*-**RuOH$_2$** − H_2O]$^{2+}$), 389.1 ([*d*-**RuOH$_2$** − H_2O + CH_3OH]$^{2+}$). ^{1}H and ^{13}C NMR, COSY, HMQC, HMBC, and ESI MS spectra are shown in Figure S2, Supporting Information.

*3. Proximal-[Ru(tpy)(L)(OH$_2$)](ClO$_4$)$_2$ (p-[**RuOH$_2$**](ClO$_4$)$_2$).* To a 200 mL flask were added *d*-[**RuOH$_2$**](NO$_3$)$_2$ (33 mg, 0.036 mmol), $NaClO_4$ (160 mg, 1.15 mmol), water (30 mL), and methanol (100 mL). The reaction mixture was irradiated under light from a 500 W xenon arc lamp equipped with a L-42 optical filter for 12h. After light irradiation, a green solid precipitated in a flask was filtered. The filtrate was additionally irradiated for 12h followed by the filtration. The combined green solid was dried in a vacuum. ***Caution!*** *Perchlorate salts of organic ligands and metal complexes are potentially explosive and must be handled with care.* Yield: 33.4 mg (92%). Anal. Calcd for *p*-[**RuOH$_2$**](ClO$_4$)$_2$·2H_2O, $C_{42}H_{30}N_8Cl_2O_9Ru·2H_2O$: C, 50.51; H, 3.43; N, 11.22. Found: C, 50.32; H, 3.49, N, 11.08. ^{1}H NMR (699.837 MHz, d_6-acetone) δ (ppm): 9.03 (d, *J* = 9.1 Hz, 1H), 8.97 (d, *J* = 8.1 Hz, 1H), 8.89 (d, *J* = 8.2 Hz, 2H), 8.85 (d, *J* = 9.1 Hz, 1H), 8.76 (d, *J* = 3.7 Hz, 1H), 8.74 (d, *J* = 9.2 Hz, 1H), 8.71 (d, *J* = 8.1 Hz, 2H), 8.59–8.52 (m, 2H), 8.50–8.39 (m, 3H), 8.04 (t, *J* = 7.8, 7.8 Hz, 2H), 8.00 (d, *J* = 5.6 Hz, 3H), 7.92 (dd, *J* = 17.0, 8.1 Hz, 2H), 7.88–7.78 (m, 5H), 7.58–7.52 (m, 1H), 7.32 (t, *J* = 6.6 Hz, 1H), 7.27 (t, *J* = 6.6 Hz, 2H). UV–vis (λ, nm (ε, 10^3 mol^{-1} L cm^{-1}) in methanol): 246 (33.0), 280 (33.0), 293 (35.0), 387 (28.0), 612 (6.2). ESI MS (solvent: methanol) (*m*/*z*): 373.1 ([*p*-**RuOH$_2$** − H_2O]$^{2+}$), 389.1, ([*p*-**RuOH$_2$** − H_2O + CH_3OH]$^{2+}$), and 402.1, ([*p*-**RuOH$_2$** − H_2O + CH_3COCH_3]$^{2+}$).^{1}H NMR, COSY, and ESI MS spectra are shown in Figure S4, Supporting Information. ^{13}C NMR, HMQC, and HMBC spectra were not obtained due to poor solubility of *p*-[**RuOH$_2$**]-(ClO$_4$)$_2$.

*4. Proximal,proximal-[Ru$_2$(tpy)$_2$(L)(μ-Cl)]Cl$_3$ (p,p-[**Ru$_2$(μ-Cl)**]Cl$_3$).* *p*-[**RuOH$_2$**](ClO$_4$)$_2$·2H_2O (139.3 mg, 0.139 mmol) was suspended in a mixed solvent of acetone (23 mL), methanol (25 mL), and water (20 mL) containing an anion-exchange resin (Amberlite IRA-400, Cl^- form, 3.5 g). The suspension was stirred for 6 h at room temperature. After the resin was removed by filtration, the filtrate was transferred to a 100 mL round-bottom flask and evaporated to ca. 10 mL. Ru(tpy)Cl_3 (65 mg, 0.147 mmol), ascorbic acid (90 mg, 0.51 mmol), LiCl (100 mg, 2.4 mmol), ethanol (20 mL), and water (20 mL) were added to the flask. The mixture was heated to evaporate to ca. 5 mL in a microwave for 40 min and then filtered. The green filtrate was purified with Sephadex LH-20 (column size 1.5 × 20 cm) three times using methanol as an eluent. The first green band was collected and evaporated to dryness. Single crystals of *p,p*-[**Ru$_2$(μ-Cl)**](BF$_4$)$_3$ suitable for X-ray crystallography were obtained by slow evaporation of ***p,p*-Ru$_2$(μ-Cl)** in water and acetone containing $NaBF_4$ and a few drops of 3 M HCl. Yield: 133.1 mg (67%). Anal. Calcd for *p,p*-[**Ru$_2$(μ-Cl)**]Cl_3·8H_2O, $C_{57}H_{39}N_{11}Cl_4Ru_2·8H_2O$: C, 50.12; H, 4.06; N, 11.28. Found: C, 49.95; H, 3.95, N, 11.21. ^{1}H NMR (699.837 MHz, CD_3OD) δ (ppm): 8.90 (d, *J* = 9.3 Hz, 2H, H_e), 8.86–8.79 (m,

DOI: 10.1021/acs.inorgchem.5b01264
Inorg. Chem. 2015, 54, 7627–7635

Scheme 2. Synthetic Scheme of a Dinuclear Ruthenium Complex, *p,p*-$Ru_2(\mu\text{-Cl})$, Using Photoisomerization of *d*-$RuOH_2$

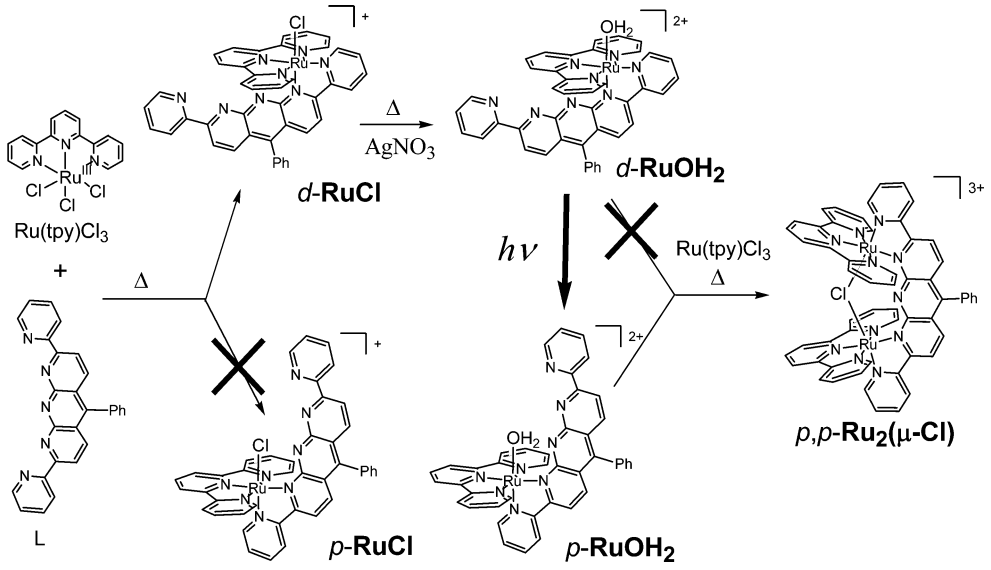

4H, H_d and H_f), 8.49 (d, J = 8.1 Hz, 4H, H_k), 8.28 (d, J = 7.9 Hz, 4H, H_l), 8.11 (t, J = 8.1 Hz, 2H, H_j), 8.06−8.02 (m, 2H, H_c), 7.97 (t, J = 7.3 Hz, 2H, H_b), 7.95−7.91 (m, 1H, H_a), 7.86−7.80 (m, 2H, H_g), 7.72 (t, J = 7.9 Hz, 4H, H_m), 7.55 (d, J = 4.9 Hz, 4H, H_o), 7.44 (d, J = 6.1 Hz, 2H, H_i), 7.13 (t, J = 6.8 Hz, 2H, H_h), 7.02 (t, J = 6.7 Hz, 4H, H_n). ^{13}C NMR (175.992 MHz, CD_3OD) δ (ppm): 162.34 (C_i), 160.82 (C_k), 159.72 (C_s), 159.29 (C_r), 159.03 (C_j), 154.82 (C_w), 154.42 (C_o), 153.84 (C_e), 139.20 (C_u), 137.61(C_g), 137.38 (C_p), 137.04 (C_m), 134.54 (C_d), 132.21 (C_c), 131.50 (C_a), 130.53 (C_b), 128.87 (C_v), 128.56 (C_n), 128.45 (C_l), 125.32 (C_f), 125.13 (C_t), 124.03 (C_q), 122.17 (C_h). UV−vis (λ, nm (ε, 10^3 mol^{-1} L cm^{-1}) in methanol): 232 (63.0), 271 (53.0), 312 (58.0), 373 (35.0), 393 (34.0), 467 (10.2), 630 (10.5). ESI MS (solvent: methanol) (m/z): 372.0 ([*p,p*-$\mathbf{Ru_2(\mu\text{-Cl})}$]$^{3+}$), 558.0 ([*p,p*-$\mathbf{Ru_2(\mu\text{-Cl})}$]$^{2+}$), 575.4 ([*p,p*-$\mathbf{Ru_2(\mu\text{-Cl})}$ + Cl$^-$]$^{2+}$). ^{1}H and ^{13}C NMR, COSY, HMQC, HMBC, and ESI MS spectra are shown in Figure S6, Supporting Information.

5. Proximal,proximal-$[Ru_2(tpy)_2(L)(\mu\text{-OH})](NO_3)_3$ (p,p-$[\mathbf{Ru_2(\mu\text{-OH})}](NO_3)_3$). *p,p*-$[\mathbf{Ru_2(\mu\text{-Cl})}]Cl_3$ (20.0 mg, 14.6 μmol) was dissolved in 0.1 M phosphate buffer (7.5 mL, pH 10.7) and left at room temperature for 14 h. To the blue-green-colored solution was added a saturated aqueous solution of $NaNO_3$ (1 mL). The green precipitate was filtered and dried in vacuum. Yield: 19.5 mg (98%). Anal. Calcd for $C_{57}H_{40}N_{14}O_{10}Ru_2{\cdot}4H_2O$: C, 50.52; H, 3.57; N, 14.47; Found: C, 50.86; H, 3.70; N, 14.28. ^{1}H NMR (699.837 MHz, 50% CD_3OD and 50% *d*-acetone) δ (ppm): 8.87−8.80 (m, 4H), 8.78 (d, J = 7.8 Hz, 2H), 8.43 (d, J = 8.1 Hz, 4H), 8.21 (d, J = 8.0 Hz, 4H), 8.06 (t, J = 8.1 Hz, 2H), 7.99−7.93 (m, 2H), 7.92−7.81 (m, 3H), 7.76−7.68 (m, 4H), 7.61 (dt, J = 8.0, 1.5 Hz, 4H), 7.31 (*d*, J = 5.6 Hz, 4H), 6.98 (ddd, J = 7.3, 6.2, 1.3 Hz, 2H), 6.79 (ddd, J = 7.1, 5.7, 1.2 Hz, 4H). UV−vis (λ, nm (ε, 10^3 mol^{-1} L cm^{-1}) in methanol): 271 (51.1), 314 (53.9) 389 (37.5), 497 (9.7), 645 (1.02). ESI MS (solvent: methanol) (m/z): 366.1 ([*p,p*-$\mathbf{Ru_2(\mu\text{-OH})}$]$^{3+}$). ^{1}H NMR, COSY, and ESI MS spectra are shown in Figure S9, Supporting Information.

6. Proximal,proximal-$[Ru_2(tpy)_2(L)(OH)(OH_2)](ClO_4)_3$ (p,p-$[\mathbf{Ru_2(OH)(OH_2)}](ClO_4)_3$). *p,p*-$[\mathbf{Ru_2(\mu\text{-Cl})}]Cl_3$ (6.9 mg, 5.0 μmol) and an aqueous solution of $AgNO_3$ (0.1 M, 0.2 mL, 20 μmol) were added in water (2.5 mL) and stirred at room temperature for 1 h. To the solution was added a 0.2 M phosphate buffer (2.5 mL, pH 7) and then heated at 70 °C for 12 h. Deposited AgCl was removed by centrifugation and filtration. *p,p*-$[\mathbf{Ru_2(OH)(OH_2)}]^{3+}$ was formed in the phosphate buffer including 5% *p,p*-$[\mathbf{Ru_2(\mu\text{-OH})}]^{3+}$ as impurity. ^{1}H NMR (699.837 MHz, 0.1 M phosphate buffer, pD = 7) δ (ppm): 8.18−7.98 (m, 16H), 7.67 (d, J = 7.4 Hz, 2H), 7.62−7.50 (m, 6H), 7.47−7.38 (m, 5H), 7.36 (d, J = 5.2 Hz, 2H), 7.14 (d, J = 6.0 Hz, 2H), 6.92−6.83 (m, 4H), 6.60 (t, J = 7.0 Hz, 2H). ^{13}C NMR (125.770 MHz, 0.1 M phosphate buffer, pD = 7) δ (ppm): 159.0, 158.2, 158.1, 158.0, 158.0, 154.3, 153.7, 153.6, 153.1, 153.0, 144.3, 138.3, 138.3. 137.6, 136.2, 135.9, 129.1, 128.7, 127.8, 127.7, 126.8, 125.5, 124.0, 123.9, 123.9, 123.6, 122.7, 116.8. ESI MS (solvent: water) (m/z): 366.1 ([*p,p*-$\mathbf{Ru_2(OH)(OH_2)}$ − H_2O]$^{3+}$) and 372.1, (*p,p*-[$\mathbf{Ru_2(OH)(OH_2)}$]$^{3+}$). ^{1}H NMR, ^{13}C NMR, and COSY, spectra are shown in Figure S10, Supporting Information. *p,p*-$[\mathbf{Ru_2(OH)(OH_2)}](ClO_4)_3$ was isolated as a perchlorate salt as follows. ***Caution!*** *Perchlorates are explosive and must be treated with great care.* *p,p*-$[\mathbf{Ru_2(\mu\text{-Cl})}]Cl_3$ (14 mg, 10.2 μmol) was dissolved in 0.1 M phosphate buffer (pH 6) and refluxed overnight to give a reddish brown solution. An aqueous solution of $NaClO_4$ was added to the solution, and the precipitate was filtered and dried. Yield: 13.6 mg (89%). Anal. Calcd for *p,p*-$[\mathbf{Ru_2(OH)(OH_2)}](ClO_4)_3{\cdot}4.5H_2O$, $C_{57}H_{42}N_{11}O_{14}Cl_3Ru_2{\cdot}4.5H_2O$: C, 45.81; H, 3.44; N, 10.31. Found: C, 45.65; H, 3.07, N, 10.20.

Measurements. NMR spectra (^{1}H, ^{13}C, ^{1}H−^{1}H COSY, ^{1}H−^{13}C HMQC, and HMBC) were recorded on a Varian 400 or 700 MHz spectrometer. ^{1}H NMR spectra were referenced using tetramethylsilane in organic solvents or sodium trimethylsilyl propanate in D_2O as an internal standard. The pD (−log[D^+]) value in D_2O was calculated using the following equation pD = pH + 0.4, where pH is the measured value by a pH meter.[37] Electrospray ionization mass spectra (ESI MS) were measured with a Waters/Micromass, ZQ 4000 spectrometer. The conditions were as follows: complex concentration, 5−50 μM; cone voltage, 20 V; capillary voltage, 3.5 kV. UV−vis absorption spectra were measured in a quartz cell with 1 cm of a light pass length using a photodiode array spectrometer (Shimadzu Multispec-1500). The electrochemical measurement was performed in a conventional single-compartment cell equipped with a glassy carbon electrode (effective area, 0.071 cm^2) as an working electrode, a saturated calomel electrode (SCE) or a mercury−mercurous sulfate electrode ($Hg/HgSO_4$) as an reference electrode, and a platinum wire counter electrode at 25 °C under an Ar atmosphere using an electrochemical analyzer (Hokuto Denko, HZ-3000 or HZ-7000). The glassy carbon working electrode was polished with polycrystalline diamonds (Struers, DP-Paste P, 1/4 μm) and rinsed with water and acetone before use. In bulk electrolysis, a platinum mesh electrode (φ = 0.7 mm, 5 mm × 10 mm) or the glassy carbon electrode was utilized as a working electrode. Gas evolved during the electrocatalysis was analyzed on a gas chromatograph (Shimadzu, GC-8A) equipped with a molecular sieve 5 Å column using argon carrier gas (flow rate is 40 cm^3 min^{-1}) at 50 °C. X-ray diffraction data of *d*-[$\mathbf{RuCl}$]$Cl{\cdot}2H_2O$ and *p,p*-$[\mathbf{Ru_2(\mu\text{-Cl})}](BF_4)_3{\cdot}H_2O$ were recorded on a Rigaku CCD diffractometer (XtaLAB mini) using graphite-monochromated Mo Kα radiation (0.71075 Å) at 25 °C. Data of *p,p*-$[\mathbf{Ru_2(\mu\text{-OH})}](ClO_4)_3{\cdot}3H_2O$ were recorded on a Bruker SMART APEXII CCD area detector diffractometer with the detector positioned at a distance of 6.0 cm

DOI: 10.1021/acs.inorgchem.5b01264
Inorg. Chem. 2015, 54, 7627−7635

from the crystal (λ = 0.71073 Å) at −173 °C. A crystal was mounted on a glass fiber. The structure was solved by direct methods and expanded using Fourier techniques. The non-hydrogen atoms were refined anisotropically. Hydrogen atoms were included but not refined except for a hydrogen atom of a hydroxo bridge. The final cycle of full-matrix least-squares refinement was based on the observed reflections ($I > 2.00\ \sigma(I)$) and variable parameters and converged with unweighted and weighted agreement factors R and R_w.

DFT Calculations. Density functional theory (DFT) calculations were performed using the Gaussian 09 package of programs.[38] Molecular structures were fully optimized using the B3LYP method, which uses hybrid Becke's three-parameter exchange functional[39] with the correlation energy functional of Lee, Yang, and Parr.[40] Calculations were performed using the standard double-ζ-type LanL2DZ basis set implemented in Gaussian 09. All DFT calculations were performed in a gas phase. The exited states were calculated by the TD-DFT method implemented in Gaussian 09. These calculations employ the hybrid B3LYP functional along with the basis sets described above. At least 250 excited states were calculated in each calculation.

RESULTS AND DISCUSSION

Synthesis of *p,p*-Ru_2XY. A multidentate bridging ligand L was utilized to construct a *proximal,proximal*-dinuclear structure (*p,p*-**Ru_2**) (see Scheme 2). The reaction of $Ru(tpy)Cl_3$ and L in ethanol selectively gave *distal*-$[Ru(tpy)(L)Cl]^+$ (*d*-**RuCl**, 59% yield), which was characterized by X-ray crystallography (Figure S1 and Tables S1 and S2, Supporting Information). The selective formation of *d*-**RuCl** is possibly due to steric hindrance of L with a chloro ligand, as is the case of *distal*-$[Ru(tpy)(pynp)Cl]^+$ formation in the reaction of $Ru(tpy)Cl_3$ and pynp.[15,16] *d*-**RuCl** was easily converted to *distal*-$[Ru(tpy)(L)OH_2]^{2+}$ (*d*-**$RuOH_2$**) by chloro subtraction with $AgNO_3$ in water (90% yield, Figure S2, Supporting Information). The thermal reaction of *d*-**$RuOH_2$** with $Ru(tpy)Cl_3$ as a second ruthenium center for dimerization in water failed to yield *p,p*-**Ru_2** species due to the steric hindrance between a tpy ligand on *d*-**$RuOH_2$** and one on $Ru(tpy)Cl_3$. Alternatively, the reaction gave a purple solution mainly containing *distal,distal*- or *distal,proximal*-dinuclear species with a Ru−carbanion bond, which were suggested by the UV−vis absorption and ESI-MS spectroscopic data (Figure S3, Supporting Information). Photoisomerization of *d*-**$RuOH_2$** to *proximal*-$[Ru(tpy)(L)OH_2]^{2+}$ (*p*-**$RuOH_2$**) should allow one to side step the steric constraint of *d*-**$RuOH_2$** for the *p,p*-**Ru_2** structure formation. The photoisomerization of *d*-**$RuOH_2$** stoichiometrically proceeded to form *p*-**$RuOH_2$** (characterized in Figure S4, Supporting Information) in D_2O/CD_3OD (4:1 vol/vol) under visible light irradiation (λ > 420 nm) (Figure S5, Supporting Information). The internal quantum yield for the photoisomerization of *d*-**$RuOH_2$** (2 mM) was shown to be 0.05% (at 520 nm) from the experiment using monochromic light (8.4 mW cm^{-2}). This value is low compared with that (0.31%) of *distal*-$[Ru(tpy)(pynp)OH_2]^{2+}$ under the same conditions. This might be due to higher contribution of nonradiative decay of the ^{3}MLCT excited state being responsible for the shorter lifetime (τ) of the ^{3}MLCT state of *d*-**$RuOH_2$**. (τ = 9 ns and less than 1 ns in H_2O at 275 K for *distal*-$[Ru(tpy)(pynp)OH_2]^{2+}$ and *d*-**$RuOH_2$**, respectively.[16]) The subsequent thermal reaction of *p*-**$RuOH_2$** with $Ru(tpy)Cl_3$ in water/ethanol (1:3 vol/vol) successfully produced the dinuclear complex with μ-Cl bridges, *proximal,proximal*-$[Ru_2(tpy)_2(L)(\mu\text{-}Cl)]^{3+}$ (*p,p*-**$Ru_2(\mu\text{-}Cl)$**) in 67% yield. *p,p*-**$Ru_2(\mu\text{-}Cl)$** was characterized by ^{1}H and ^{13}C NMR, 2D-NMR, and ESI MS spectroscopies (Figure S6, Supporting Information) and X-ray crystallography (Figure 1, Tables S1 and S2, Supporting Information). ^{1}H and ^{13}C NMR spectra exhibited C_{2v} symmetry of *p,p*-**$Ru_2(\mu\text{-}Cl)$** with equivalence of two tpy ligands in CD_3OD, which is supported by density functional theory (DFT) calculations (Figure S7, Supporting Information).

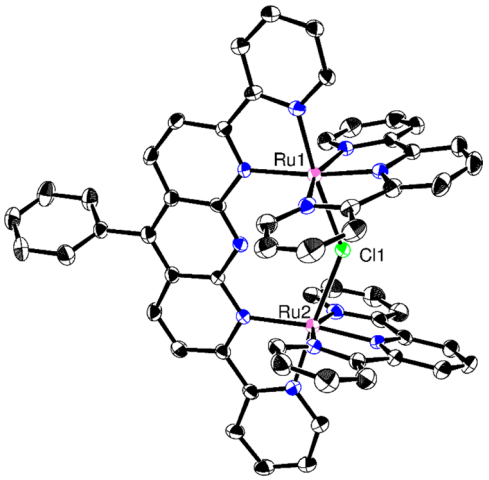

Figure 1. ORTEP view of *p,p*-**$[Ru_2(\mu\text{-}Cl)](BF_4)_3\cdot H_2O$** (30% probability). Counteranions and a solvent are omitted for clarity.

Figure 1 shows an Oak Ridge thermal ellipsoid plot (ORTEP) drawing of *p,p*-**$Ru_2(\mu\text{-}Cl)$**. The Ru−Cl bond length between the Ru centers and the chloro bridge of *p,p*-**$Ru_2(\mu\text{-}Cl)$** is 2.4838 Å on average, which is longer than that (2.4060(11) Å) of *d*-**RuCl** by 0.0778 Å (Table S2, Supporting Information). The angle among Ru1−Cl1−Ru2 is 139.62(7)°, and the distance between the Ru centers is 4.662 Å. The larger angle of Ru1−Cl1−Ru2 and the longer Ru−Ru distance are notable as a characteristic core structure of *p,p*-**$Ru_2(\mu\text{-}Cl)$** when compared with the core structure (Ru−Cl bond length, 2.4466(7) Å; Ru−Cl−Ru angle, 104.77(4)°; Ru−Ru distance, 3.876 Å) of a dinuclear ruthenium complex with a bis(2-pyridyl)-3.5-pyrazolate bridge reported by Llobet et al.[24]

Bridge-Exchange Reactions of *p,p*-Ru_2XY. On the ^{1}H NMR spectrum of *p,p*-**$Ru_2(\mu\text{-}Cl)$** in D_2O (pD = 10.7), the signal at 8.75 ppm for *p,p*-**$Ru_2(\mu\text{-}Cl)$** gradually decreased with an increase of the signal of 8.91 ppm, and this change was completed in 1 day at room temperature (Figure S8, Supporting Information). The ^{1}H NMR spectrum of the completed solution showed C_{2v} symmetry similar to that of *p,p*-**$Ru_2(\mu\text{-}Cl)$**. The ESI MS spectrum of the species isolated from the completed solution gave a signal at m/z = 366.1 as a trication species, being in agreement with the simulated isotopic patterns of $[Ru_2(tpy)_2(L)(\mu\text{-}OH)]^{3+}$ (Figure S9C, Supporting Information). Crystals afforded from the reacted solution were characterized by X-ray crystallographic analysis (Tables S1 and S2, Supporting Information), and the structure derived from X-ray diffraction data is shown by the ORTEP drawing in Figure 2. The angle (156.5(2)°) among Ru1−O1−Ru2 is smaller than that (165.4(3)°) of the blue dimer of μ-O-dinuclear ruthenium(III) complex[41] but significantly larger than that (139.62(7)°) among Ru1−Cl1−Ru2 of *p,p*-**$Ru_2(\mu\text{-}Cl)$**. The Ru−O bond length (2.145 Å in average) between the Ru centers and μ-OH for *p,p*-**$Ru_2(\mu\text{-}OH)$** is longer than that (1.869 Å) for the blue dimer[41] due to the μ-OH bridge. Consequently, the distance (4.193 Å) between the Ru centers for *p,p*-**$Ru_2(\mu\text{-}OH)$** is longer than that (3.709 Å) of the blue dimer. The distance between the Ru centers can be changed

DOI: 10.1021/acs.inorgchem.5b01264
Inorg. Chem. 2015, 54, 7627−7635

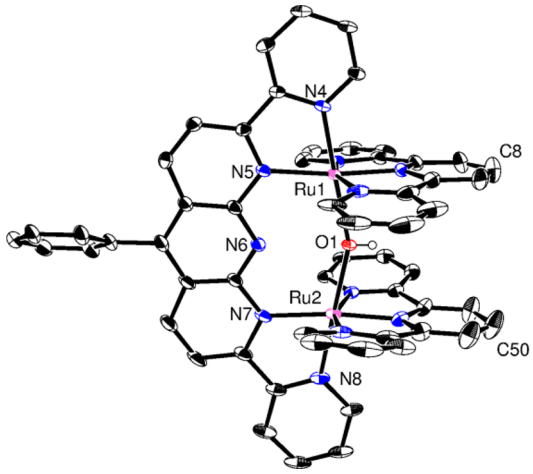

Figure 2. ORTEP view of *p,p*-[$\mathbf{Ru_2(\mu\text{-}OH)}$] $(ClO_4)_3{\cdot}3H_2O$ (30% probability). Counteranions and solvents are omitted for clarity.

from 4.193 to 4.662 Å by μ-OH and μ-Cl bridges for the series of *p,p*-$\mathbf{Ru_2XY}$ complexes, respectively. The flexible L-based backbone of *p,p*-$\mathbf{Ru_2XY}$ complexes is responsible for the chelate-exchange reaction. Thus, the μ-Cl bridge of *p,p*-$\mathbf{Ru_2(\mu\text{-}Cl)}$ is substituted with solvent water to form *p,p*-$\mathbf{Ru_2(\mu\text{-}OH)}$ in weakly basic conditions (Scheme 3). *p,p*-$\mathbf{Ru_2(\mu\text{-}OH)}$ is unusual

Scheme 3. Reversible Bridge-Exchange Reactions Among *p,p*-$\mathbf{Ru_2(\mu\text{-}Cl)}$, *p,p*-$\mathbf{Ru_2(\mu\text{-}OH)}$, and *p,p*-$\mathbf{Ru_2(OH)(OH_2)}$[a]

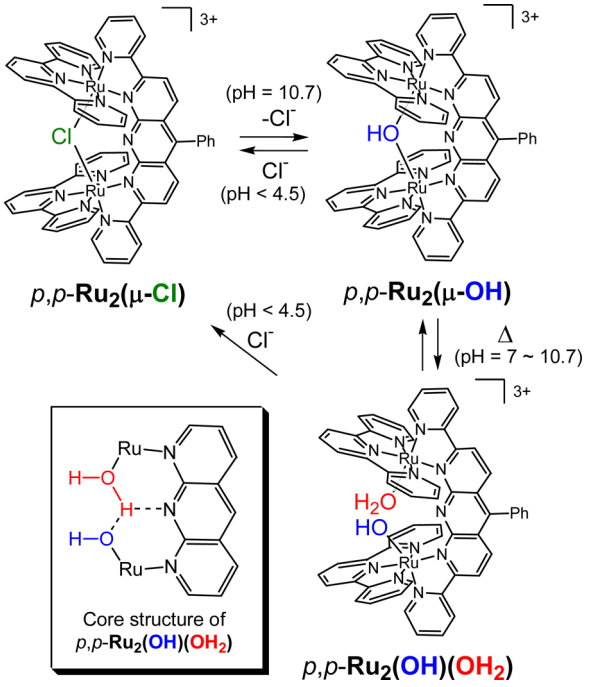

[a]Inset shows the core structure image of *p,p*-$\mathbf{Ru_2(OH)(OH_2)}$.

as a polypyridyl dinuclear ruthenium complexes with a μ-OH ligand formed stably in a mild aqueous medium,[42,43] irrespective of a large number of μ-O-type dinuclear ruthenium complexes reported previously.[44−49] The detailed structure of *p,p*-$\mathbf{Ru_2(\mu\text{-}OH)}$ could provide significant insight into control of the basicity of μ-O ligands for polypyridyl dinuclear ruthenium complexes.

When *p,p*-$\mathbf{Ru_2(\mu\text{-}OH)}$ was heated at 70 °C in phosphate buffer solutions (pD = 7.0−10.7) for 12 h, the signal at 8.91 ppm for *p,p*-$\mathbf{Ru_2(\mu\text{-}OH)}$ decreased in the ^{1}H NMR spectrum and instead the new signal at 8.30 ppm increased to attain a 1:9 ratio in signal areas between 8.91 and 8.30 ppm. This suggests that the formed species (for 8.30 ppm) exists in equilibrium with *p,p*-$\mathbf{Ru_2(\mu\text{-}OH)}$. The ESI MS spectrum of the reacted solution exhibited signals at m/z = 366.1 and 372.1 as trication species, in agreement with the simulated isotopic patterns of $[Ru_2(tpy)_2(L)(OH)]^{3+}$ and $[Ru_2(tpy)_2(L)(OH)(OH_2)]^{3+}$, respectively (Figure 3). These signals shifted to m/z = 366.4 and

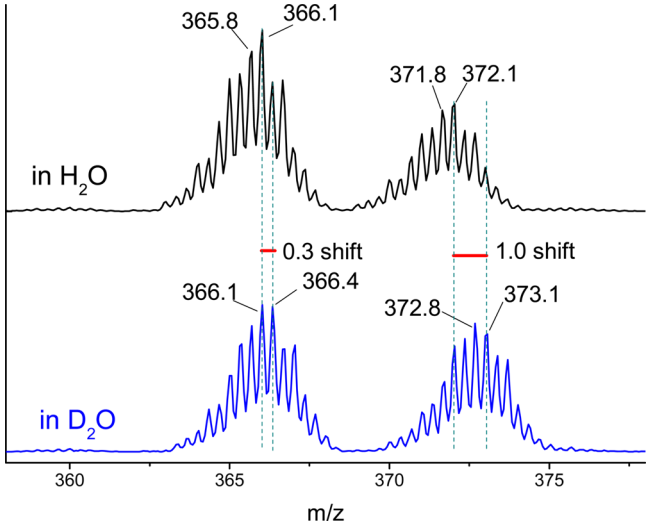

Figure 3. ESI MS spectra of *p,p*-$[\mathbf{Ru_2(OH)(OH_2)}](NO_3)_3$ in H_2O (top) and D_2O (bottom).

373.1 by 0.3 and 1.0 in D_2O, showing that one and three proton(s) of the former and latter species are exchangeable with solvent water, respectively. These results indicate that *p,p*-$\mathbf{Ru_2(\mu\text{-}OH)}$ converts to *proximal,proximal*-$[Ru_2(tpy)_2(L)(OH)(OH_2)]^{3+}$ (*p,p*-$\mathbf{Ru_2(OH)(OH_2)}$) in water under neutral and weakly basic conditions (Scheme 3). The ^{1}H NMR spectrum showed C_2 symmetry of *p,p*-$\mathbf{Ru_2(OH)(OH_2)}$ with nonequivalence of two tpy ligands in D_2O (Figure S10, Supporting Information). This is ascribed to the distorted L chelate and the hydrogen-bond interaction (HO···H_2O) between O of hydroxo and H of aquo ligands. The H atom shared by oxoes of aquo and hydroxo ligands is supposed to be further stabilized by hydrogen-bond interaction with the central N of the anthyridine moiety (inset in Scheme 3). These are supported by the optimized structure of DFT calculations (Figure S7, Supporting Information). Irrespective of the lower symmetry, *p,p*-$\mathbf{Ru_2(OH)(OH_2)}$ is predominantly formed in neutral and weakly basic conditions due to the specially stabilized core structure by the multiple hydrogen-bond interactions among aquo, hydroxo, and backbone L ligands. When the aqueous solution of *p,p*-$\mathbf{Ru_2(\mu\text{-}OH)}$ or *p,p*-$\mathbf{Ru_2(OH)(OH_2)}$ goes back to pH < 4.5, *p,p*-$\mathbf{Ru_2(\mu\text{-}Cl)}$ was immediately and stoichiometrically formed in the presence of equivalent of Cl ions. The reversible bridge-exchange reactions thus occur among *p,p*-$\mathbf{Ru_2(\mu\text{-}Cl)}$, *p,p*-$\mathbf{Ru_2(\mu\text{-}OH)}$, and *p,p*-$\mathbf{Ru_2(OH)(OH_2)}$, as illustrated in Scheme 3.

Electronic Structures of *p,p*-$\mathbf{Ru_2XY}$. The UV−vis absorption spectrum of *p,p*-$\mathbf{Ru_2(\mu\text{-}Cl)}$ in methanol provides absorption maxima at 312, 373, 393, 467, and 630 nm (Figure

DOI: 10.1021/acs.inorgchem.5b01264
Inorg. Chem. 2015, 54, 7627−7635

4, black). The absorption bands at 310, 372, and 393 nm were assigned to be a $\pi-\pi^*$ transition of L according to the

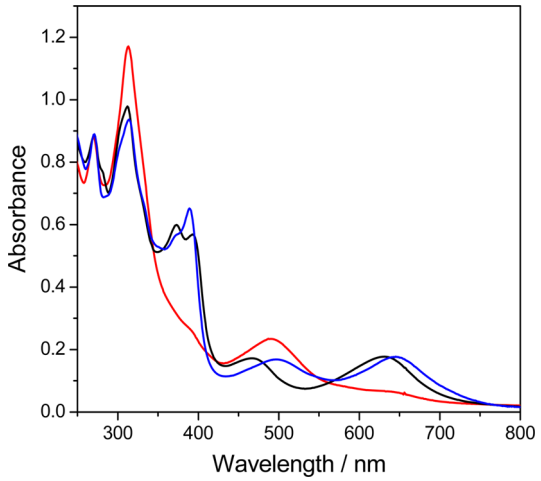

Figure 4. Absorption spectra of *p,p*-$\mathbf{Ru_2(\mu\text{-}Cl)}$ (black) in methanol, *p,p*-$\mathbf{Ru_2(\mu\text{-}OH)}$ (blue) in methanol, and *p,p*-$\mathbf{Ru_2(OH)(OH_2)}$ (red) in a 0.1 M phosphate buffer at pH 7.

literature;[50] the bands at 630 and 467 nm were assigned to MLCT transitions from Ru to L and to both tpy and L based on time-dependent DFT calculations, respectively (Figures S11 and S12 and Table S3, Supporting Information). The absorption spectra (Figure 4, blue) of *p,p*-$\mathbf{Ru_2(\mu\text{-}OH)}$ in methanol showed red shifts of the absorption bands (assigned in the same manner as *p,p*-$\mathbf{Ru_2(\mu\text{-}Cl)}$) to 645 and 497 nm due to the destabilized level of the Ru center by μ-OH substitution (Figures S11 and S13 and Table S4, Supporting Information). The absorption spectra (Figure 4, red) of *p,p*-$\mathbf{Ru_2(OH)(OH_2)}$ (90% yield) in 0.1 M phosphate buffer (pH 7) gave a shoulder at 670 nm and a peak at 490 nm, which are assigned to be MLCT transitions from Ru to L and to both tpy and L, respectively (Figures S11 and S14 and Table S5, Supporting Information).

Electrochemical Properties of *p,p*-$\mathbf{Ru_2(OH)(OH_2)}$. The cyclic voltammogram (CV) of *p,p*-$\mathbf{Ru_2(OH)(OH_2)}$ gave two oxidation waves at 0.64 and 0.79 V vs a saturated calomel electrode (SCE) and two reduction waves at 0.24 and 0.68 V in a potential range of 0−1.0 V vs SCE (inset of Figure 5). The potentiostatic electrolysis in a *p,p*-$\mathbf{Ru_2(OH)(OH_2)}$ solution (0.5 mM, 0.8 mL, pH = 6.0) at 0.75 V required 71 mC (1.8 equiv of the complex amount) to complete the electrochemical reaction, indicating that the first oxidation at 0.64 V is the 2-electron process most likely to form the Ru^{III}:Ru^{III} state. The UV−vis absorption spectral change during electrolysis clearly showed an absorbance decrease at 490 nm and concomitant appearance of a new absorption band at 699 nm with isosbestic points at 289, 375, 427, and 618 nm (Figure 6). The solution after the electrolysis was EPR silent at 77 K and provided new signals in a wide region of a chemical shift on the ^{1}H NMR spectrum (Figure S15, Supporting Information). The observed diamagnetic properties could be explained by antiferromagnetic interaction between the Ru^{III} centers. The antiferromagnetic coupling of the Ru^{III}:Ru^{III} state was reported for a similar dinuclear ruthenium complex.[51] The redox wave at 0.64 V is pH dependent (slope = 28 mV/pH) near the neutral conditions, suggesting the 1-proton-coupled 2-electron oxidaiton process of Ru^{II}−OH:Ru^{II}−OH_2 to Ru^{III}−OH:Ru^{III}−OH.

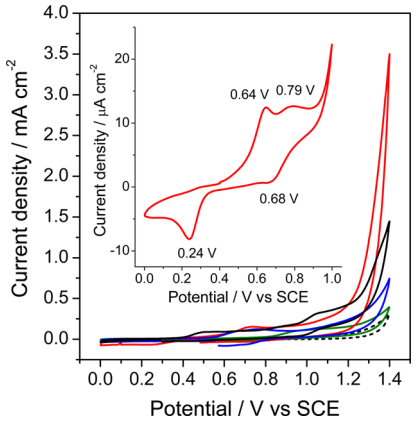

Figure 5. Cyclic voltammograms of 1 mM *p,p*-$\mathbf{Ru_2(OH)(OH_2)}$ (red), *d*-$\mathbf{RuOH_2}$ (blue), *p,p*-$\mathbf{Ru_2(\mu\text{-}Cl)}$ (green), and blank (black dots) in a 0.1 M phosphate buffer using a glassy carbon electrode (pH 6.0, scan rate 50 mV s^{-1}). CV of *p,p*-$\mathbf{Ru_2(\mu\text{-}OH)}$ (black) was measured at pH 9.0 because it gradually converts to *p,p*-$\mathbf{Ru_2(\mu\text{-}Cl)}$ at acidic conditions. (Inset) CV of 0.5 mM *p,p*-$\mathbf{Ru_2(OH)(OH_2)}$ in a 0.1 M phosphate buffer (pH 7.0) (scan rate 20 mV s^{-1}).

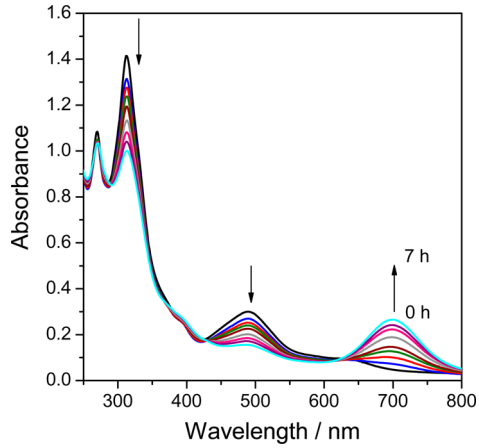

Figure 6. UV−vis absorption spectra change of a *p,p*-$\mathbf{Ru_2(OH)(OH_2)}$ solution during bulk electrolysis at 0.75 V vs SCE (pH = 6.0, 0.1 M phosphate buffer).

The back electrolysis at 0 V exhibited a reverse absorption spectral change to recover Ru^{II}−OH:Ru^{II}−OH_2, indicating that the reduction wave at 0.24 V is due to the rereduction of Ru^{III}−OH:Ru^{III}−OH to Ru^{II}−OH:Ru^{II}−OH_2. The significantly large peak separation between the oxidation (0.64 V) and the reduction waves (0.24 V) based on the Ru^{II}−OH:Ru^{II}−OH_2/Ru^{III}−OH:Ru^{III}−OH redox pair could be explained by either some chemical reactions or conformational changes involved in the redox reaction. The oxidation wave at 0.79 V is also pH dependent (slope = 20 mV/pH), and the charge amount (102 mC) is comprarable with that (117 mC) at 0.64 V for the Ru^{II}−OH:Ru^{II}−OH_2/Ru^{III}−OH:Ru^{III}−OH redox. This suggests that the oxidation wave at 0.79 V and the corresponding reduction wave at 0.68 V are assigned to the 1-proton-coupled 2-electron redox process of a Ru^{III}−OH:Ru^{III}−OH/Ru^{IV}=O:Ru^{IV}−OH redox.

The CV of *p,p*-$\mathbf{Ru_2(OH)(OH_2)}$ extended to 1.4 V (Figure 5) provided a precipitous and high anodic current above 1.2 V vs SCE due to water oxidation, showing that *p,p*-$\mathbf{Ru_2(OH)(OH_2)}$ works for electrocatalytic water oxidation. The current value reached 3.5 mA cm^{-2} (0.31 mA cm^{-2} for a blank without

DOI: 10.1021/acs.inorgchem.5b01264
Inorg. Chem. 2015, 54, 7627−7635

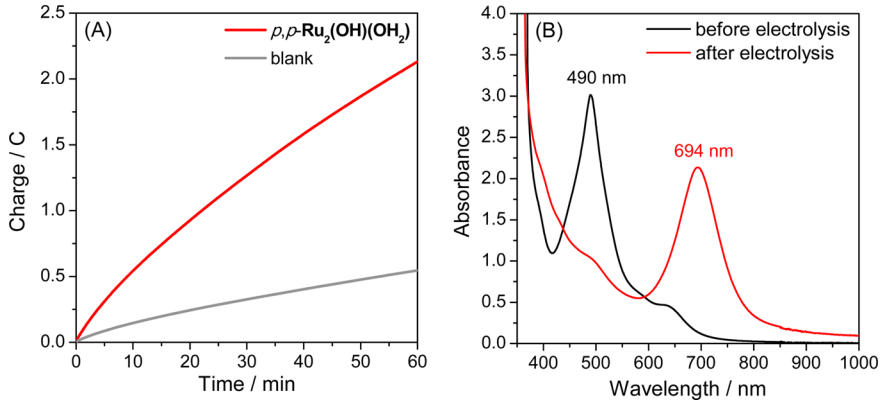

Figure 7. (A) Current−time curve during bulk electrolysis of 0.2 mM *p,p*-$\mathbf{Ru_2(OH)(OH_2)}$ (red), and blank without the complex (gray) at 1.30 V vs SCE in a 0.1 M phosphate buffer (pH = 7.0, 3.0 mL). A platinum mesh electrode was used as a working electrode. (B) UV−vis absorption spectra of 0.2 mM *p,p*-$\mathbf{Ru_2(OH)(OH_2)}$ before (black) and after (red) bulk electrolysis.

complex) at 1.4 V, which was 4.8 and 9.2 times higher than those of *d*-$\mathbf{RuOH_2}$ and *p,p*-$\mathbf{Ru_2(\mu\text{-}Cl)}$. CV of *p,p*-$\mathbf{Ru_2(\mu\text{-}OH)}$ was measured at pH = 9.0 because it gradually converts to *p,p*-$\mathbf{Ru_2(\mu\text{-}Cl)}$ at acidic conditions. The current value (3.5 mA cm^{-2} at pH = 6.0) of *p,p*-$\mathbf{Ru_2(OH)(OH_2)}$ was much higher than that (1.4 mA cm^{-2} at pH = 9.0) of *p,p*-$\mathbf{Ru_2(\mu\text{-}OH)}$ even under thermodynamically unfavorable pH conditions. These results suggest that the *p,p*-$\mathbf{Ru_2}$ structure with aquo and hydroxo ligands is important for efficient electrocatalytic water oxidation.

Electrocatalytic Water Oxidation in a Homogeneous Solution. A chemical water oxidation technique using a Ce(IV) oxidant has been extensively employed to examine activities of water oxidation catalysts in homogeneous solution. However, it is limited under only strongly acidic conditions because precipitation of $Ce(OH)_4$ is formed above pH = 3.5. O_2 evolution was not observed in an aqueous *p,p*-$\mathbf{Ru_2(OH)(OH_2)}$ solution at pH = 1 in a chemical water oxidation experiment using a Ce(IV) oxidant. This is due to the stability of *p,p*-$\mathbf{Ru_2(OH)(OH_2)}$ in acidic conditions; *p,p*-$\mathbf{Ru_2(OH)(OH_2)}$ immediately coverts to less catalytically active *p,p*-$\mathbf{Ru_2(\mu\text{-}Cl)}$ in the presence of the slight Cl^- ions as a counter, or *p,p*-$\mathbf{Ru_2(OH)(OH_2)}$ is destructured without Cl^- ions less than pH = 4.5. The electrochemical technique is useful to study water oxidation catalysis under neutral conditions. The bulk electrolysis was conducted in a phosphate buffer solution of *p,p*-$\mathbf{Ru_2(OH)(OH_2)}$ (0.2 mM, pH = 7.0) at 1.3 V vs SCE. The significantly high charge amount (2.1 C) relative to the blank (0.55 C) without the complex was observed (Figure 7A), and 4.2 μmol (Faradaic efficiency 76%) of O_2[52] was evolved during the 1 h electrolysis (1.0 μmol of O_2 was evolved in blank electrolysis). The O_2 amount (3.2 μmol) evolved in the electrocatalysis by *p,p*-$\mathbf{Ru_2(OH)(OH_2)}$ for 1 h corresponds to 5.3 equiv of the total *p,p*-$\mathbf{Ru_2(OH)(OH_2)}$ amount (0.6 μmol) in the electrolyte solution, which significantly ensures the catalyst turnover (more than unity) in electrochemical water oxidation. The UV−vis absorption spectrum of the electrolyte solution after electrolysis showed an intense band at 694 nm (Figure 7B), which is nearly the same as the characteristic absorption band (699 nm) of the Ru^{III}−OH:Ru^{III}−OH species. This observation suggests that the Ru^{III}−OH:Ru^{III}−OH species is a resting state in the catalytic cycle. For the proposed electrocatalytic cycle for water oxidation under neutral conditions, Ru^{II}−OH:Ru^{II}−OH_2 is electrochemically oxidized via Ru^{III}−OH:Ru^{III}−OH and Ru^{IV}=O:Ru^{IV}−OH most possibly to the Ru^{V}=O:Ru^{V}=O state, which could oxidize water to O_2 with regeneration of the Ru^{III}−OH:Ru^{III}−OH state.

Isotope Effects on Electrocatalytic Water Oxidation. It is of significance to reveal the mechanism of the O−O bond formation by *p,p*-$\mathbf{Ru_2(OH)(OH_2)}$, involving whether there is nucleophilic attack of H_2O on a Ru^{V}=O center (WNA mechanism)[23,53−55] or intramolecular O−O coupling of the adjacent Ru^{V}=O centers (IOC mechanism).[25,56] The ^{18}O-labeling experiment using $H_2{}^{18}O$ is a general method to provide insight into the mechanism of O−O bond formation in a chemical water oxidation system.[25,56−58] In this experiment, exchange of aquo ligands on catalyst complexes with solvent $H_2{}^{18}O$ must be sufficiently slow compared with a time scale of O_2 detection to elucidate the distribution of the ^{18}O-labeled O_2 evolution. The effectual distribution data could be difficult to be provided by the ^{18}O-labeling experiment in the present electrocatalytic system, because a longer time scale (of hours) for O_2 detection is required compared with the exchange of aquo ligands on *p,p*-$\mathbf{Ru_2(OH)(OH_2)}$ with solvent water due to the restricted electrochemical cell volume. Alternatively, we propose different experiments to provide insight into mechanism of O−O bond formation based on an isotope effect of H/D. The electron transfer processes on the electrode are postulated to be fast relative to the chemical process including O−O bond formation in the electrocatalytic cycle because they are diffusion-controlled processes of redox species in the electrolyte solution at sufficiently higher applied potential. If this is not the case, the electron transfer processes could be isotope effectless in H_2O and D_2O media. The nucleophilic attack of water is concerted with proton transfer from the water to adjacent water molecules or adequate bases in the WNA mechanism,[59] whereas proton transfer is not involved in coupling of adjacent Ru^{V}=O centers in the IOC mechanism. It is hypothesized that the isotope effect on O−O bond formation could be observed for the WNA mechanism but not for the IOC mechanism. The bulk electrolysis was conducted in solutions of *d*-$\mathbf{RuOH_2}$ and *p,p*-$\mathbf{Ru_2(OH)(OH_2)}$ in H_2O and D_2O media. For *d*-$\mathbf{RuOH_2}$, the charge amount (Q_H = 20.2 ± 0.02 mC) required for the electrolysis in H_2O was higher than that (Q_D =11.9 ± 0.01 mC) in D_2O by a factor of 1.7 ± 0.04 (Figure S16, Supporting Information, and Table 1). The value of Q_H/Q_D = 1.7 is regarded as a significant isotope effect on the electrocatalysis, compared with the blank experiment without complex (Q_H/Q_D = 1.1 ± 0.20). This is consistent with the proton transfer-concerted O−O bond

DOI: 10.1021/acs.inorgchem.5b01264
Inorg. Chem. 2015, 54, 7627−7635

Table 1. Summary of the Charge Amount Data Required for Electrochemical Water Oxidation in a 0.1 M Phosphate Buffer (pH or pD = 7.0)[a]

complexes	Q_H/mC	Q_D/mC	Q_H/Q_D
p,p-**Ru$_2$(OH)(OH$_2$)**	28.5 ± 1.10	25.8 ± 0.02	1.1 ± 0.04
d-**RuOH$_2$**	20.2 ± 0.02	11.9 ± 0.01	1.7 ± 0.04
blank	7.9 ± 1.16	7.1 ± 0.17	1.1 ± 0.20

[a]Applied potential is 1.30 V vs SCE. A glassy carbon electrode was used as a working electrode.

formation by the WNA mechanism as it is for mononuclear ruthenium complex catalysts.[23,55] In contrast, for *p,p*-**Ru$_2$(OH)(OH$_2$)**, the charge amount (Q_H = 28.5 ± 1.10) in H_2O was close to that (Q_H = 25.8 ± 0.02) in D_2O, and the isotope effect (Q_H/Q_D = 1.1 ± 0.04) is comparable with the blank experiment (Q_H/Q_D = 1.1). This suggests that the O−O bond formation mechanism for *p,p*-**Ru$_2$(OH)(OH$_2$)** is different from the WNA mechanism. The smaller isotope effect could be explained by a proton-nonconcerted chemical reaction process in the electrocatalytic cycle, and O−O bond formation by the IOC mechanism is likely for *p,p*-**Ru$_2$(OH)(OH$_2$)**. However, any spectroscopic evidence for the IOC mechanism is not attained yet.

CONCLUSION

We demonstrated the unique strategic synthesis of a new series of *p,p*-**Ru$_2$XY** complexes using photoisomerization of a mononuclear ruthenium(II) aquo complex. The unusual bridge-exchange reactions yield derivatives of *p,p*-**Ru$_2$(μ-Cl)**, *p,p*-**Ru$_2$(μ-OH)**, and *p,p*-**Ru$_2$(OH)(OH$_2$)** with μ-Cl, μ-OH, as well as hydroxo and aquo ligands on X and Y sites of *p,p*-**Ru$_2$XY**, respectively. *p,p*-**Ru$_2$(OH)(OH$_2$)** works more efficiently for electrocatalytic water oxidation compared with a similar mononuclear complex *d*-**RuOH$_2$**, *p,p*-**Ru$_2$(μ-Cl)**, and *p,p*-**Ru$_2$(μ-OH)**, showing that the *p,p*-**Ru$_2$** core structure with aquo and hydroxo ligands is important for efficient electrocatalytic water oxidation. The smaller isotope effect on electrocatalytic water oxidation in H_2O and D_2O media for *p,p*-**Ru$_2$(OH)(OH$_2$)** relative to *d*-**RuOH$_2$** suggests the O−O bond formation mechanism for *p,p*-**Ru$_2$(OH)(OH$_2$)** is different from the WNA mechanism as it is for mononuclear ruthenium complexes including *d*-**RuOH$_2$**.

ASSOCIATED CONTENT

Supporting Information

1H and 13C NMR, COSY, HMQC, HMBC, and ESI MS spectroscopic and X-ray crystallographic data, DFT calculations, and data of bulk electrolysis. The Supporting Information is available free of charge on the ACS Publications website at DOI: 10.1021/acs.inorgchem.5b01264.

AUTHOR INFORMATION

Corresponding Author

*Phone/Fax: +81-25-262-6790. E-mail: yagi@eng.niigata-u.ac.jp.

Notes

The authors declare no competing financial interest.

ACKNOWLEDGMENTS

This work was supported by the JST PRESTO program, JSPS KAKENHI Grant Numbers 24107003 and 24350028.

REFERENCES

(1) Kalyanasundaram, K. *Coord. Chem. Rev.* **1982**, *46*, 159.
(2) Juris, A.; Balzani, V.; Barigelletti, F.; Campagna, S.; Belser, P.; Von Zelewsky, A. *Coord. Chem. Rev.* **1988**, *84*, 85.
(3) Balzani, V.; Juris, A. *Coord. Chem. Rev.* **2001**, *211*, 97.
(4) Kirch, M.; Lehn, J.-M.; Sauvage, J.-P. *Helv. Chim. Acta* **1979**, *62*, 1345.
(5) Nicewicz, D. A.; MacMillan, D. W. C. *Science* **2008**, *322*, 77.
(6) Durham, B.; Walsh, J. L.; Carter, C. L.; Meyer, T. J. *Inorg. Chem.* **1980**, *19*, 860.
(7) Pinnick, D. V.; Durham, B. *Inorg. Chem.* **1984**, *23*, 1440.
(8) Hecker, C. R.; Fanwick, P. E.; McMillin, D. R. *Inorg. Chem.* **1991**, *30*, 659.
(9) Howerton, B. S.; Heidary, D. K.; Glazer, E. C. *J. Am. Chem. Soc.* **2012**, *134*, 8324.
(10) Durham, B.; Wilson, S. R.; Hodgson, D. J.; Meyer, T. J. *J. Am. Chem. Soc.* **1980**, *102*, 600.
(11) Porter, G. B.; Sparks, R. H. *J. Photochem.* **1980**, *13*, 123.
(12) Padhi, S. K.; Fukuda, R.; Ehara, M.; Tanaka, K. *Inorg. Chem.* **2012**, *51*, 5386.
(13) Rachford, A. A.; Rack, J. J. *J. Am. Chem. Soc.* **2006**, *128*, 14318.
(14) Miyazaki, S.; Kojima, T.; Fukuzumi, S. *J. Am. Chem. Soc.* **2008**, *130*, 1556.
(15) Yamazaki, H.; Hakamata, T.; Komi, M.; Yagi, M. *J. Am. Chem. Soc.* **2011**, *133*, 8846.
(16) Hirahara, M.; Ertem, M. Z.; Komi, M.; Yamazaki, H.; Cramer, C. J.; Yagi, M. *Inorg. Chem.* **2013**, *52*, 6354.
(17) NOTE: The *proximal*/*distal*-isomers were defined by the structural configuration between a naphthyridine moiety of pynp and an aquo ligand.
(18) Cady, C. W.; Crabtree, R. H.; Brudvig, G. W. *Coord. Chem. Rev.* **2008**, *252*, 444.
(19) Concepcion, J. J.; Jurss, J. W.; Brennaman, M. K.; Hoertz, P. G.; Patrocinio, A. O. T.; Iha, N. Y. M.; Templeton, J. L.; Meyer, T. J. *Acc. Chem. Res.* **2009**, *42*, 1954.
(20) Yamazaki, H.; Shouji, A.; Kajita, M.; Yagi, M. *Coord. Chem. Rev.* **2010**, *254*, 2483.
(21) Hirahara, M.; Shoji, A.; Yagi, M. *Eur. J. Inorg. Chem.* **2014**, *2014*, 595.
(22) Gersten, S. W.; Samuels, G. J.; Meyer, T. J. *J. Am. Chem. Soc.* **1982**, *104*, 4029.
(23) Concepcion, J. J.; Jurss, J. W.; Templeton, J. L.; Meyer, T. J. *J. Am. Chem. Soc.* **2008**, *130*, 16462.
(24) Sens, C.; Romero, I.; Rodriguez, M.; Llobet, A.; Parella, T.; Benet-Buchholz, J. *J. Am. Chem. Soc.* **2004**, *126*, 7798.
(25) Bozoglian, F.; Romain, S.; Ertem, M. Z.; Todorova, T. K.; Sens, C.; Mola, J.; Rodriguez, M.; Romero, I.; Benet-Buchholz, J.; Fontrodona, X.; Cramer, C. J.; Gagliardi, L.; Llobet, A. *J. Am. Chem. Soc.* **2009**, *131*, 15176.
(26) Sander, A. C.; Maji, S.; Francàs, L.; Böhnisch, T.; Dechert, S.; Llobet, A.; Meyer, F. *ChemSusChem* **2015**, *8*, 1697.
(27) Boyer, J. L.; Polyansky, D. E.; Szalda, D. J.; Zong, R.; Thummel, R. P.; Fujita, E. *Angew. Chem., Int. Ed.* **2011**, *50*, 12600.
(28) Kärkäs, M. D.; Åkermark, T.; Johnston, E. V.; Karim, S. R.; Laine, T. M.; Lee, B.-L.; Åkermark, T.; Privalov, T.; Åkermark, B. *Angew. Chem., Int. Ed.* **2012**, *51*, 11589.
(29) Duan, L.; Bozoglian, F.; Mandal, S.; Stewart, B.; Privalov, T.; Llobet, A.; Sun, L. *Nat. Chem.* **2012**, *4*, 418.
(30) Duan, L.; Araujo, C. M.; Ahlquist, M. S. G.; Sun, L. *Proc. Natl. Acad. Sci. U. S. A.* **2012**, *109*, 15584.
(31) Jiang, Y.; Li, F.; Zhang, B.; Li, X.; Wang, X.; Huang, F.; Sun, L. *Angew. Chem., Int. Ed.* **2013**, *52*, 3398.
(32) Masaoka, S.; Sakai, K. *Chem. Lett.* **2009**, *38*, 182.
(33) Yagi, M.; Tajima, S.; Komi, M.; Yamazaki, H. *Dalton Trans.* **2011**, *40*, 3802.
(34) Wada, T.; Tsuge, K.; Tanaka, K. *Angew. Chem., Int. Ed.* **2000**, *39*, 1479.
(35) Sullivan, B. P.; Calvert, J. M.; Meyer, T. J. *Inorg. Chem.* **1980**, *19*, 1404.

DOI: 10.1021/acs.inorgchem.5b01264
Inorg. Chem. 2015, 54, 7627−7635

(36) Murray, T. J.; Zimmerman, S. C.; Kolotuchin, S. V. *Tetrahedron* **1995**, *51*, 635.
(37) Glasoe, P. K.; Long, F. A. *J. Phys. Chem.* **1960**, *64*, 188.
(38) Frisch, M. J.; et al.*Gaussian 09*; Gaussian, Inc.: Wallingford, CT, 2009.
(39) Becke, A. D. *J. Chem. Phys.* **1993**, *98*, 5648.
(40) Lee, C.; Yang, W.; Parr, R. G. *Phys. Rev. B: Condens. Matter Mater. Phys.* **1988**, *37*, 785.
(41) Gilbert, J. A.; Eggleston, D. S.; Murphy, W. R.; Geselowitz, D. A.; Gersten, S. W.; Hodgson, D. J.; Meyer, T. J. *J. Am. Chem. Soc.* **1985**, *107*, 3855.
(42) Llobet, A.; Doppelt, P.; Meyer, T. J. *Inorg. Chem.* **1988**, *27*, 514.
(43) Di Giovanni, C.; Vaquer, L.; Sala, X.; Benet-Buchholz, J.; Llobet, A. *Inorg. Chem.* **2013**, *52*, 4335.
(44) Weaver, T. R.; Meyer, T. J.; Adeyemi, S. A.; Brown, G. M.; Eckberg, R. P.; Hatfield, W. E.; Johnson, E. C.; Murray, R. W.; Untereker, D. *J. Am. Chem. Soc.* **1975**, *97*, 3039.
(45) Gersten, S. W.; Samuels, G. J.; Meyer, T. J. *J. Am. Chem. Soc.* **1982**, *104*, 4029.
(46) Lebeau, E. L.; Adeyemi, S. A.; Meyer, T. J. *Inorg. Chem.* **1998**, *37*, 6476.
(47) Sasaki, Y.; Suzuki, M.; Nagasawa, A.; Tokiwa, A.; Ebihara, M.; Yamaguchi, T.; Kabuto, C.; Ochi, T.; Ito, T. *Inorg. Chem.* **1991**, *30*, 4903.
(48) Wang, W.-Z.; Liu, X.; Liao, D.-Z.; Jiang, Z.-H.; Yan, S.-P.; Wang, G.-L. *Inorg. Chem. Commun.* **2002**, *5*, 1007.
(49) Yoshida, M.; Kondo, M.; Nakamura, T.; Sakai, K.; Masaoka, S. *Angew. Chem.* **2014**, *126*, 11703.
(50) Djurdjevic, S.; Leigh, D. A.; McNab, H.; Parsons, S.; Teobaldi, G.; Zerbetto, F. *J. Am. Chem. Soc.* **2007**, *129*, 476.
(51) Roeser, S.; Ertem, M. Z.; Cady, C.; Lomoth, R.; Benet-Buchholz, J.; Hammarström, L.; Sarkar, B.; Kaim, W.; Cramer, C. J.; Llobet, A. *Inorg. Chem.* **2012**, *51*, 320.
(52) NOTE: Faradaic efficiency is 80% when taking the charge amount for formation of the Ru^{III}–Ru^{III} resting state into account.
(53) Wasylenko, D. J.; Ganesamoorthy, C.; Henderson, M. A.; Koivisto, B. D.; Osthoff, H. D.; Berlinguette, C. P. *J. Am. Chem. Soc.* **2010**, *132*, 16094.
(54) Kimoto, A.; Yamauchi, K.; Yoshida, M.; Masaoka, S.; Sakai, K. *Chem. Commun.* **2012**, *48*, 239.
(55) Concepcion, J. J.; Jurss, J. W.; Norris, M. R.; Chen, Z. F.; Templeton, J. L.; Meyer, T. J. *Inorg. Chem.* **2010**, *49*, 1277.
(56) Romain, S.; Bozoglian, F.; Sala, X.; Llobet, A. *J. Am. Chem. Soc.* **2009**, *131*, 2768.
(57) Yamada, H.; Siems, W. F.; Koike, T.; Hurst, J. K. *J. Am. Chem. Soc.* **2004**, *126*, 9786.
(58) Cape, J. L.; Siems, W. F.; Hurst, J. K. *Inorg. Chem.* **2009**, *48*, 8729.
(59) Chen, Z. F.; Concepcion, J. J.; Hu, X. Q.; Yang, W. T.; Hoertz, P. G.; Meyer, T. J. *Proc. Natl. Acad. Sci. U. S. A.* **2010**, *107*, 7225.

DOI: 10.1021/acs.inorgchem.5b01264
Inorg. Chem. 2015, 54, 7627−7635